Relative resistance to slow inactivation of human cardiac Na+ channel hNav1.5 is reversed by lysine or glutamine substitution at V930 in D2-S6

Jessica Hotard Chancey, Penny E. Shockett and John P. O'Reilly

Am J Physiol Cell Physiol 293:1895-1905, 2007. First published Oct 10, 2007;
doi:10.1152/ajpcell.00377.2007

Am J Physiol Cell Physiol 293: C1895–C1905, 2007.
First published October 10, 2007; doi:10.1152/ajpcell.00377.2007.

Relative resistance to slow inactivation of human cardiac Na^+ channel $hNa_v1.5$ is reversed by lysine or glutamine substitution at V930 in D2-S6

Jessica Hotard Chancey, Penny E. Shockett, and John P. O'Reilly

Department of Biological Sciences, Southeastern Louisiana University, Hammond, Louisiana

Submitted 23 August 2007; accepted in final form 4 October 2007

Chancey JH, Shockett PE, O'Reilly JP. Relative resistance to slow inactivation of human cardiac Na^+ channel $hNa_v1.5$ is reversed by lysine or glutamine substitution at V930 in D2-S6. *Am J Physiol Cell Physiol* 293: C1895–C1905, 2007. First published October 10, 2007; doi:10.1152/ajpcell.00377.2007.—Transmembrane segment 6 is implicated in slow inactivation (SI) of voltage-gated Na^+ channels (Na_vs). To further study its role and understand differences between SI phenotypes of different Na_v isoforms, we analyzed several domain 2-segment 6 (D2-S6) mutants of the human cardiac $hNa_v1.5$, which is relatively resistant to SI. Mutants were examined by transient HEK cell transfection and patch-clamp recording of whole cell Na^+ currents. Substitutions with lysine (K) included N927K, V930K, and L931K. We show recovery from short (100 ms) depolarization to 0 mV in N927K and L931K is comparable to wild type, whereas recovery in V930K is delayed and biexponential, suggesting rapid entry into a slow-inactivated state. SI protocols confirm enhanced SI phenotype (rapid development, hyperpolarized steady state, slowed recovery) for V930K, contrasting with the resistant phenotype of wild-type $hNa_v1.5$. This enhancement, not found in N927K or L931K, suggests that the effect in V930K is site specific. Glutamine (Q) substituted at V930 also exhibits an enhanced SI phenotype similar to that of V930K. Therefore, K or Q substitution eliminates $hNa_v1.5$ resistance to SI. Alanine (A) or cysteine (C) substitution at V930 shows no enhancement of SI, and in fact, V930A and V930C, as well as L931K, exhibit a resistance to SI, demonstrating that characteristics of specific amino acids (e.g., size, hydrophobicity) differentially affect SI gating. Thus V930 in D2-S6 appears to be an important structural determinant of SI gating in $hNa_v1.5$. We suggest that conformational change involving D2-S6 is a critical component of SI in Na_vs, which may be differentially regulated between isoforms by other isoform-specific determinants of SI phenotype.

sodium channel; voltage gating; site-directed mutagenesis

VOLTAGE-GATED Na^+ channels (Na_vs) are transmembrane proteins composed of an α-subunit with four homologous domains (D1–D4), each with six transmembrane segments (S1–S6), and accessory β-subunits. Heterologous expression of the α-subunit is sufficient for the key components of voltage-gated channel function, i.e., activation, ion selectivity, ion flow, and inactivation (12, 23, 43). Na_vs respond to depolarization of the membrane by opening a Na^+ ion-selective pore that permits the flow of Na^+ ions down their electrochemical gradient into the cell. This response of Na_vs to membrane depolarization is called activation and is the mechanism responsible for the rapid upstroke of the action potential in most excitable cells, including cardiac cells in the human heart.

In response to the same stimulus (i.e., membrane depolarization), Na_vs enter a nonconducting state called inactivation, in which they usually remain until the membrane is repolarized. This process can happen within milliseconds, as in classic fast inactivation, or on a time scale of seconds, as in slow inactivation. The molecular components for fast inactivation gating have been described (20, 32, 40), whereas the gating mechanism for slow inactivation remains elusive. Interestingly, studies have found that these two processes are distinct at the molecular level. For example, fast inactivation can be eliminated with intracellular perfusion of protease (36) or by amino acid substitutions in the proposed fast-inactivation gate, the D3-D4 linker (10). However, neither of these treatments eliminates slow inactivation, suggesting that slow inactivation involves molecular mechanisms different from those of fast inactivation (10, 36).

Currently, there are two hypotheses to explain the molecular mechanisms responsible for slow inactivation in Na_vs. The first is that slow inactivation is due to conformational change in P-loops between S5 and S6 of Na_vs. This may be a mechanism similar to that occurring in C-type inactivation in K^+ channels (15, 19, 25, 31). Support for this hypothesis comes from studies showing that methanethiosulfonate (MTS) modification in the D3 P-loop of the cysteine-substituted mutant F1236C in rat skeletal muscle $Na_v1.4$ ($rNa_v1.4$) increases with some depolarization protocols (27), and that disulfide bond formation between cysteines is enhanced during slow inactivation in the double-cysteine mutant K1237C + W1531C in $rNa_v1.4$ (4). In addition, a mutation in the P-loop of D1 (W402C in $rNa_v1.4$) partially disrupts slow inactivation (3). These studies suggest that conformational changes in the P-loops are associated with slow inactivation. However, another study using the SCAM (substituted cysteine accessibility method) technique found no changes in accessibility in the P-loops during Na_v slow inactivation, suggesting little conformational change in this region (41).

The second hypothesis poses that slow inactivation involves conformational changes in the putative pore-lining S6 transmembrane segments of the four domains: D1-S6, D2-S6, D3-S6, and D4-S6 (7, 28, 30, 44, 55, 56). Support for this hypothesis comes from studies showing that substitution of alanine for native asparagine (N434A) in D1-S6 of $rNa_v1.4$ enhances slow inactivation (56), substitution of different residues in the same isoform at V787 in D2-S6 produces enhancement of or resistance to slow inactivation (30), slow inactivation in rat brain Na_v isoform $rNa_v1.2$ can be enhanced or diminished with substitutions at N1466 in D3-S6 (7), and tryptophan or lysine substitution in D4-S6 in S1759W or S1759K in the human cardiac Na_v isoform hNav1.5 produces

Address or reprint requests and other correspondence: J. P. O'Reilly, Dept. of Biological Sciences, SLU 10736, Southeastern Louisiana Univ., Hammond, LA 70402 (e-mail: joreilly@selu.edu).

The costs of publication of this article were defrayed in part by the payment of page charges. The article must therefore be hereby marked "*advertisement*" in accordance with 18 U.S.C. Section 1734 solely to indicate this fact.

a biphasic effect on slow inactivation (55). In addition, molecular movement during Na$_v$ slow inactivation was demonstrated by MTS modification at V1583C in D4-S6 in the closed state, but not the slow-inactivated state (44), and at V787C of D2-S6 in rNa$_v$1.4 and the homologous mutant V930C in hNa$_v$1.5 in the slow-inactivated state, but not the closed state (28, 30). Together, these data suggest that dynamic molecular rearrangement or movement in the S6 segments lining the inner pore of Na$_v$s is required during slow inactivation. It should be emphasized that putative roles for P-loops and S6 segments in slow inactivation are not mutually exclusive, and interaction between these regions during slow inactivation has been proposed (42, 55).

Of interest for this study is that different Na$_v$ isoforms exhibit different slow inactivation phenotypes. For example, cardiac hNa$_v$1.5 is relatively resistant to slow inactivation compared with skeletal muscle rNa$_v$1.4 (29, 35). Although a single point mutation in the D2 P-loop (V754I) converts the hNa$_v$1.4 steady-state slow inactivation phenotype to that of hNa$_v$1.5 (46), partially explaining the difference in slow inactivation phenotype between these two isoforms (47), the precise molecular mechanisms that underlie the differences of entry into and recovery from the slow-inactivated state are unknown. Studies with Na$_v$ chimeras using domains from hNa$_v$1.5 and rNa$_v$1.4 demonstrated that if D1 and D2 (or D1, D2, and D3) are from rNa$_v$1.4, then entry into, steady state, and recovery from slow inactivation resemble that of rNa$_v$1.4 (29) suggesting that D1 and D2 play a role in determining slow inactivation phenotype. Interestingly, molecular rearrangement during slow inactivation at V930 in D2-S6 of cardiac hNa$_v$1.5, albeit requiring more time, can be detected as in V787C in rNa$_v$1.4 (28, 30), suggesting that there are some shared mechanistic components of slow inactivation in Na$_v$ isoforms that differ in overall slow inactivation phenotypes (29, 35). These results demonstrate that comparative studies between different Na$_v$s provide important information about kinetic processes that can vary among isoforms (11, 26, 37).

Understanding unique molecular mechanisms of kinetic function in Na$_v$ isoforms is particularly pertinent to understanding diseases involving heritable Na$_v$ mutations that disrupt these processes (6, 21, 48). For example, Brugada syndrome (BrS) is a cardiac disease in which there is an increased risk for ventricular fibrillation and a high incidence of sudden death, usually at rest or during sleep, in patients with normal heart structure (1, 5). Approximately 20% of BrS cases are caused by mutations in the gene encoding the α-subunit (*SCN5A*) of the cardiac hNav1.5 (2, 22). These mutations have been described as "loss-of-function" mutations, because they consistently alter Na$_v$ expression and/or gating such that there is a reduction in Na^+ current (48). Interestingly, several of the mutations that have been characterized in BrS exhibit enhanced slow inactivation (16, 38, 39, 45, 49, 50). Enhanced slow inactivation is a good candidate for a molecular mechanism that would present as the loss of Na$_v$ function seen in BrS and other cardiac disorders (48), and therefore, increasing our understanding of what controls this process in hNa$_v$1.5 has important clinical significance.

In the present study, we focused our attention on hNa$_v$1.5 because slow inactivation has not been extensively characterized in this isoform. In addition, hNa$_v$1.5 is relatively resistant to slow inactivation compared with other isoforms such as skeletal muscle Na$_v$1.4, a physiologically relevant characteristic important for maintaining Na$_v$ availability during prolonged cardiac action potentials. We initially studied residue V930 in D2-S6 of hNa$_v$1.5 because we found earlier (30) that lysine substitution at the homologous site (V787) in the rat skeletal muscle Na$_v$ isoform rNa$_v$1.4 greatly enhanced slow inactivation. Given the inherent resistance to slow inactivation required for normal cardiac function, we asked whether the analogous mutation (i.e., V930K) would similarly influence slow inactivation in the hNa$_v$1.5 isoform.

In this study we studied several lysine (K) substitutions in D2-S6 (N927K, V930K, and L931K) and several different amino acid substitutions for the native valine at residue V930 (alanine in V930A, cysteine in V930C, and glutamine in V930Q). We found that substitution of lysine or glutamine in V930K or V930Q, respectively, greatly enhanced all measures of slow inactivation phenotype, whereas N927K, L931K, V930A, and V930C did not.

Based on the results of this study, we suggest that *1*) V930 in D2-S6 plays an important role in slow inactivation gating in hNa$_v$1.5; *2*) reversal of resistance to slow inactivation in V930K and V930Q is site specific and residue specific; *3*) the greater size and hydrophilic nature of K and Q compared with the native valine plays a role in the enhancement of slow inactivation in V930K and V930Q; and *4*) hNa$_v$1.5 and rNa$_v$1.4 share the requirement for molecular movement in D2-S6 for slow inactivation gating, despite differences in their overall slow inactivation phenotype. Considering this work in conjunction with previous studies in both isoforms, we propose that varied abilities to undergo conformational changes involving V930 in D2-S6 can partially explain differences in slow inactivation phenotype observed in different Na$_v$ isoforms.

MATERIALS AND METHODS

Na^+ Channel Mutant Construction and Transient Transfection of cDNA Clones

Site-directed mutagenesis of wild-type human cardiac muscle hNa$_v$1.5 (12) was carried out as described previously (28). Mutagenic oligonucleotides (Operon Biotechnologies, Huntsville, AL) included: N927K-top, GTTATGGTCATTGGCAAGCTTGTGGTCCTGAATCTC; N927K-bot, GAGATTCAGGACCACAAGCTTGCCAATGACCATAAC; L931K-top, GTCATTGGCAACCTTGTGGTCAAGAATCTCTTCCTGGCCTTG; L931K-bot, CAAGGCCAGGAAGAGATTCTTGACCACAAGGTTGCCAATGAC; V930R-top, GTCATTGGCAACCTTGTGCGCCTGAATCTCTTCCTGGCC; V930R-bot, GGCCAGGAAGAGATTCAGGCGCACAAGGTTGCCAATGAC; V930Q-top, GTCATTGGCAACCTTGTGCAGCTGAATCTCTTCCTGGCC; V930Q-bot, GGCCAGGAAGAGATTCAGCTGCACAAGGTTGCCAATGAC; V930A-top, GTCATTGGCAACCTTGTGGCCCTGAATCTCTTCCTGGCC; V930A-bot, GGCCAGGAAGAGATTCAGGGCCACAAGGTTGCCAATGAC; V930D-top, GTCATTGGCAACCTTGTGGACCTGAATCTCTTCCTGGCC; and V930D-bot, GGCCAGGAAGAGATTCAGGTCCACAAGGTTGCCAATGAC. The V930K and V930C mutants were provided by Dr. Sho-Ya Wang (SUNY Albany, Albany, NY). cDNA clones (5–20 μg) of wild-type hNa$_v$1.5 and hNa$_v$1.5 mutants were expressed from pcDNA1-Amp (Invitrogen, Carlsbad, CA) after transient transfection into human embryonic kidney (HEK) cells by calcium phosphate precipitation (13) as previously described (28, 29). The transfection included 1–2 μg of a cDNA clone encoding cell surface antigen CD8 (OriGene, Rockville, MD).

Recording Techniques

We used standard patch-clamp techniques (14) to record whole cell peak Na^+ current (I_{Na}) from transiently transfected HEK cells. Recordings were performed at room temperature (21 ± 1°C) without correction for the liquid junction potential. Activation (conductance-voltage, *G-V*) and steady-state fast inactivation (h_∞) curves were obtained ~5 min after rupture of the membrane. Recording micropipettes (Drummond Scientific, Broomall, PA) were pulled on a model P-97 Flaming-Brown puller (Sutter Instruments, Novato, CA). Pipette resistances ranged from 0.5 to 2.0 MΩ when measured in our solutions. The extracellular recording solution was (in mM) 65 NaCl, 85 choline-Cl, 2 $CaCl_2$, and 10 HEPES, titrated to pH 7.4 with tetramethylammonium-OH. The intracellular solution in the pipette was (in mM) 100 NaF, 30 NaCl, 10 EGTA, and 10 HEPES, titrated to pH 7.2 with CsOH. These solutions create an outward Na^+ gradient and an outward Na^+ current at the test pulse of +50 mV, reducing potential problems associated with space clamp or series resistance errors (9). Series resistance was compensated at 80%, resulting in voltage errors of <5 mV. Linear leak subtraction based on five hyperpolarizing pulses was used for all recordings. Any endogenous K^+ currents were blocked with Cs^+ in the pipette, and HEK cells express no native Ca^{2+} current (43). Cells were selected for recording based on positive immunoreaction with anti-CD8 Dynabeads (Dynal Biotech, Lake Success, NY).

Electrophysiology Protocols

Activation and fast inactivation. The holding potential (V_{hold}) was −160 mV (−180 for V930K because of the enhanced voltage dependence of inactivation for this mutant). A test pulse to +50 mV (4 ms) was used to record peak available Na^+ current (I_{Na}). Activation curves were obtained from the peak current recorded with pulses from V_{hold} to voltages over the range of −100 to + 50 mV in 10-mV increments. Steady-state fast inactivation (h_∞) was determined with a test pulse to +50 mV to record I_{Na} following a conditioning prepulse (100 ms) from V_{hold} to −30 mV in 10-mV increments. The half-maximal potential ($V_{½}$) and slope factor (k) for activation and steady-state fast inactivation were obtained from a fit of the mean data with a Boltzmann function.

Recovery from short depolarizations. Recovery from short depolarizations was determined with the following double-pulse protocol: a step to 0 mV for 4 or 100 ms, a step to V_{hold} for variable recovery times (1 ms to 30 s), and then a test pulse to +50 mV (4 ms). The peak current recorded with the test pulse was normalized to I_{Na} obtained with a test pulse after 30 s at V_{hold}. The mean data were fit with a single-exponential function. Recovery curves for a 100-ms step to 0 mV for V930K and V930Q were fit with a double-exponential function.

Slow inactivation phenotype. Three protocols were used to determine slow inactivation phenotype (28, 29): *1*) development of slow inactivation, *2*) voltage dependence of steady-state slow inactivation (s_∞), and *3*) recovery from slow inactivation.

DEVELOPMENT OF SLOW INACTIVATION. Voltage was stepped from V_{hold} to 0 mV for various times (1 ms to 60s for hNa$_v$1.5, 50 ms to 60s for N927K, L931K, V930A, and V930C, and 1 ms to 30 s for V930K), stepped to V_{hold} for 50 ms to allow recovery from fast inactivation, and then stepped to +50 mV (4 ms) to record I_{Na}. I_{Na} was normalized to the initial value recorded with a test pulse from V_{hold} before the start of the protocol. Mean data were fit with a single- (hNa$_v$1.5, N927K, L931K, V930A, and V930C) or double-exponential function (V930K and V930Q).

STEADY-STATE SLOW INACTIVATION (S_∞). A 60-s prepulse (10 s for V930K) was stepped in 20-mV increments between V_{hold} and 0 mV, followed by a 50-ms step to V_{hold} (to allow recovery from fast inactivation) and then a 4-ms test pulse to +50 mV to record I_{Na}. I_{Na} was normalized to I_{Na} recorded with a test pulse from −160 or −180 mV (V930K) before the protocol. $V_{½}$ and slope factor k were obtained from a fit of the mean data with a Boltzmann function.

RECOVERY FROM SLOW INACTIVATION. Voltage was stepped to 0 mV for 60 s (10 s for V930K), stepped to V_{hold} for various times (50 ms to 30 or 60 s), and then a subsequent 4-ms test pulse to +50 mV. I_{Na} was normalized to I_{Na} obtained after maximum time at V_{hold}. Data were fit with a single-exponential function (V930K and V930Q with a double exponential). Data were collected and filtered at 5 kHz with an Axopatch 200B amplifier using pClamp software (Axon Instruments, Foster City, CA). Curve fits and data analysis were performed with pClamp and Origin software (Microcal Software, Northampton, MA). Differences from wild type were considered significant at $P < 0.05$ (ANOVA). Grouped data are presented as means ± SE.

RESULTS

Steady-State Fast Inactivation and Activation in the Lysine-Substituted Mutants N927K, V930K, and L931K

We studied V930K in hNa$_v$1.5 to determine whether this isoform was sensitive to lysine substitution at this residue as has been observed with the homologous mutation in rNa$_v$1.4 (30). To determine whether any effects observed in V930K were site specific, we studied N927K (about 1 turn of the α-helix away) and L931K (adjacent to V930), which had been shown to express adequately in the analogous mutants in the rNa$_v$1.4 isoform (51).

The activation curve of the mutant N927K was not statistically different from that of wild-type hNa$_v$1.5 (Fig. 1*A*, Table 1). However, the activation curves for L931K ($V_{½} = -27.4 \pm 1.2$ mV, $P < 0.001$) and V930K ($V_{½} = -34.7 \pm 1.6$ mV, $P < 0.05$) were depolarized, and the curve for V930K was also less steep ($k = 14.6 \pm 1.6$, $P < 0.001$) compared with that for hNa$_v$1.5 ($V_{½} = -41.7 \pm 1.1$ mV, $k = 10.5 \pm 1.0$; Fig. 1*A*, Table 1). Sample traces from the activation protocol are shown in Fig. 2.

For steady-state fast inactivation (h_∞), N927K was hyperpolarized ($V_{½} = -86.3 \pm 0.7$ mV, $P < 0.01$), L931K was depolarized ($V_{½} = -67.6 \pm 0.9$ mV, $P < 0.001$), and V930K was hyperpolarized and less steep ($V_{½} = -96.7 \pm 1.8$ mV, $P < 0.001$; $k = 12.5 \pm 1.1$, $P < 0.001$) compared with hNa$_v$1.5 ($V_{½} = -80.7 \pm 0.7$ mV, $k = 6.8 \pm 0.4$; Fig. 1*B*, Table 1).

Recovery From Short Depolarizations in N927K, V930K, and L931K

Short depolarizations result in Na$_v$s opening and then entering the fast-inactivated state. We studied the recovery from the fast-inactivated state by stepping to 0 mV for 4 or 100 ms and then stepping to V_{hold} for variable amounts of time, using a test pulse to +50 mV to measure available (i.e., noninactivated) current. Recovery from a 4-ms depolarization was not statistically different between wild type and the lysine-substituted mutants V930K and L931K (Fig. 3*A*, Table 1). Compared with wild type ($\tau = 2.1 \pm 0.1$ ms), N927K required a slightly but significantly longer recovery time ($\tau = 2.8 \pm 0.3$ ms, $P < 0.05$; Fig. 3*A*, Table 1).

The recovery curves from a 100-ms depolarization for wild type, N927K, and L931K had similar time constants, ranging from 2.6 to 4.1 ms (Fig. 3*B*, Table 1). However, V930K exhibited a different time course of recovery from a 100-ms depolarization. The recovery in V930K was delayed and biex-

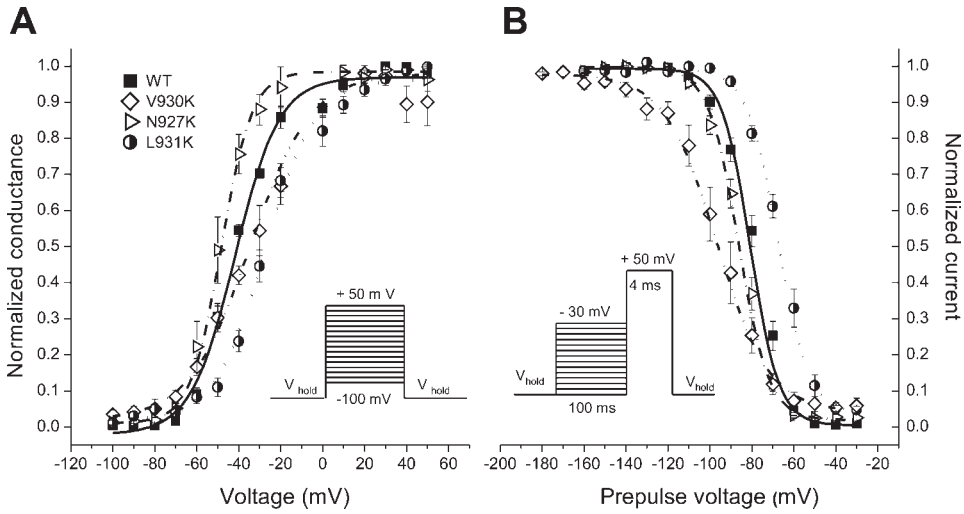

Fig. 1. Activation (*G-V*) and steady-state fast inactivation (h_∞) curves in the human cardiac Na^+ channel hNav1.5 wild type (WT) and lysine-substituted mutants N927K, V930K, and L931K. Mean data were fit with a Boltzmann function. *A*: the activation curve for N927K was similar to that for WT. Activation in L931K was right-shifted, and that in V930K was depolarized and less steep than that in WT. *B*: the h_∞ curve for N927K was hyperpolarized, that for L931K was depolarized, and that for V930K was hyperpolarized and less steep compared with that for WT. Data are presented in Table 1.

ponential with $\tau 1 = 5.3 \pm 0.5$ ms and $\tau 2 = 3.9 \pm 0.2$ s (Fig. 3*B*, Table 1). These results suggest that this mutant is entering into two distinct inactivation states within the 100-ms depolarization.

Slow Inactivation Phenotype in N927K, V930K, and L931K

The recovery profile from a 100-ms depolarization in V930K suggested that this mutant was rapidly entering a slow inactivation state. We used our slow inactivation protocols to characterize the phenotype of the three lysine-substituted mutants (see MATERIALS AND METHODS and Fig. 4*D*).

For development of slow inactivation in N927K and L931K, time constants from the exponential fits of the data were not significantly different from wild type, although slow inactivation in L931K was less complete (Fig. 4*A*, Table 2). For example, after a 60-s depolarization at 0 mV, L931K showed ~17% slow inactivation, whereas the wild type was ~45% inactivated (Fig. 4*A*). In sharp contrast to N927K and L931K, the mutant V930K exhibited a dramatic enhancement of slow inactivation. Development of slow inactivation in this mutant was biexponential with a rapid onset ($\tau 1 = 67.2 \pm 6.3$ ms) and greater in magnitude than the others, reaching almost 80% slow inactivation after a 10-s depolarization at 0 mV (Fig. 4*A*, Table 2).

The s_∞ curve for the mutant N927K was not significantly different from wild type (Fig. 4*B*, Table 2). The $V_{½}$ of the s_∞ curve for L931K also did not differ significantly from that of the wild type. However, this mutant underwent less slow inactivation than the wild type (Fig. 4*B*, Table 2). In contrast, V930K showed a dramatic hyperpolarized shift of −88 mV in the s_∞ curve ($V_{½} = -155.6 \pm 7.5$ mV, $P < 0.001$) compared with wild type ($V_{½} = -67.5 \pm 3.2$ mV) or the other mutants (Fig. 4*B*, Table 2).

Recovery from slow inactivation followed a pattern similar to development and a steady state of slow inactivation. Recovery in hNa$_v$1.5, N927K, and L931K were similar, although L931K recovered from less slow inactivation than the others. In V930K, recovery from slow inactivation was much slower and biexponential, with a $\tau 2 > 6$ s, whereas wild type and the other mutants recovered on a time scale of hundreds of milliseconds (Fig. 4*C*, Table 2).

Steady-State Fast Inactivation and Activation in Mutants With Substitutions at V930

To determine whether the enhanced slow inactivation phenotype of V930K was residue specific to lysine substitution at this site, we studied various other amino acid substitutions at

Table 1. *Fast gating properties for hNa$_v$1.5 and mutant channels*

	Activation		Steady-State Fast Inactivation		Fast Recovery (4 ms)	Fast Recovery (100 ms)
	$V_{½}$, mV	k	$V_{½}$, mV	k	τ, ms	τ, ms
hNa$_v$1.5	−41.7±1.1 (10)	10.5±1.0	−80.7±0.7 (17)	6.8±0.4	2.1±0.1 (14)	2.6±0.1 (14)
N927K	−48.5±1.3 (6)	7.3±0.7	−86.3±0.7† (10)	7.2±0.4	2.8±0.3* (8)	4.1±0.3† (8)
V930K	−34.7±1.6* (6)	14.6±1.6‡	−96.7±1.8‡ (6)	12.5±1.1‡	1.7±0.1 (5)	5.3±0.5 (39%) 3,901±174 (63%) (9)
L931K	−27.4±1.2‡ (10)	11.8±0.7	−67.6±0.9‡ (10)	7.3±0.6	1.7±0.1 (9)	2.6±0.2 (8)
V930A	−32.7±0.4‡ (28)	11.2±0.6	−91.3±0.6‡ (19)	7.6±0.3‡	3.1±0.2† (18)	3.4±0.2‡ (17)
V930C	−35.4±0.6‡ (20)	11.1±0.6	−81.9±0.5 (17)	7.4±0.3†	2.4±0.2 (8)	2.6±0.3 (9)
V930Q	−39.1±0.7* (14)	9.9±0.7	−81.6±1.0 (12)	7.6±0.5*	3.0±0.2† (10)	5.6±0.3 (66%) 42.9±4.6 (34%) (11)

Activation (conductance-voltage relation) and steady-state fast inactivation curves were fit with a Boltzmann function. Half-maximal potential ($V_{½}$) and slope factor (k) of activation and steady-state inactivation are presented as means ± SE; numbers in parentheses are the number of cells recorded. Recovery from short (4 or 100 ms) depolarization curves were fit with a single-exponential function, except for V930K and V930Q recovering from a 100-ms depolarization, which required a double-exponential fit, and time constants (τ) of recovery are means ± SE; percentages indicate component of fit. *$P < 0.05$; †$P < 0.01$; ‡$P < 0.001$ compared with wild-type human cardiac Na^+ channel hNa$_v$1.5.

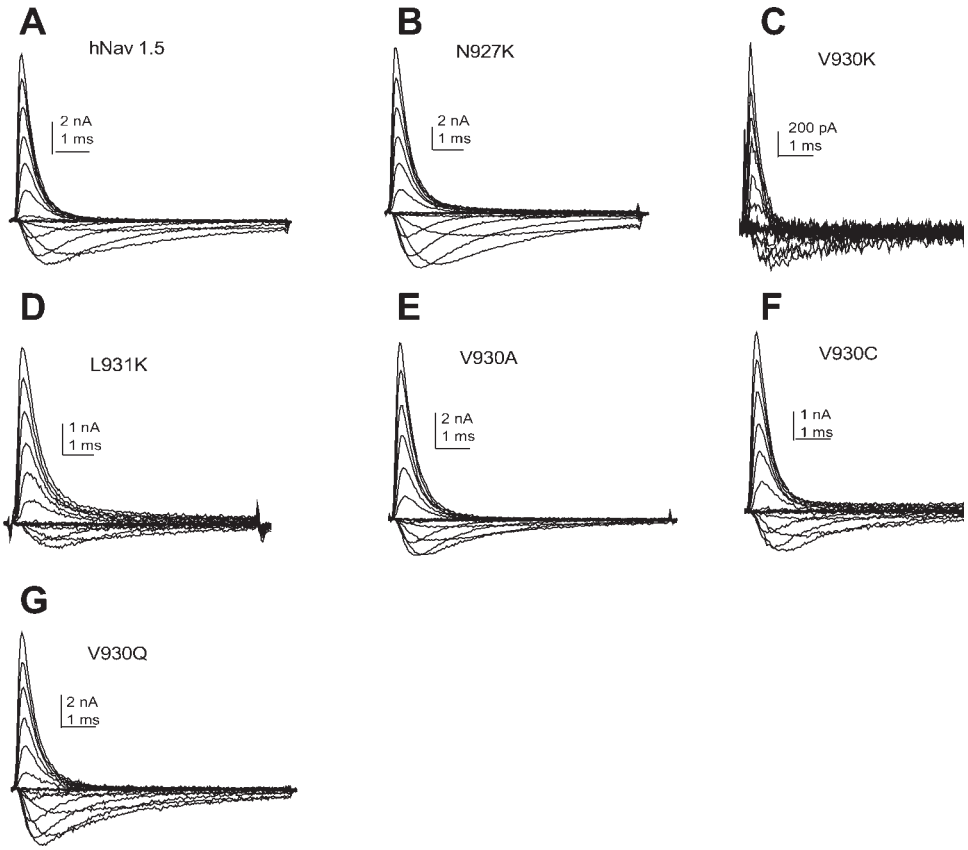

Fig. 2. Sample traces of Na^+ currents recorded from hNa$_v$1.5 (*A*), N927K (*B*), V930K (*C*), L931K (*D*), V930A (*E*), V930C (*F*), and V930Q (*G*) using the activation protocol (see description in Fig. 1*A*).

the V930 residue. These mutants included V930A (alanine), V930C (cysteine), V930D (aspartate), V930R (arginine), and V930Q (glutamine), which were chosen based on characteristics such as hydrophobicity and size. V930D and V930R did not express sufficient current for analysis, whereas three mutants expressed well: V930A, V930C, and V930Q. The activation curves in all of these mutants were shifted in the depolarized direction ($V_{½}$ = −32.7 ± 0.4 mV, $P < 0.001$; −35.4 ± 0.6 mV, $P < 0.001$; and −39.1 ± 0.7 mV, $P < 0.05$, respectively) compared with wild type (−41.7 ± 1.1 mV; Fig. 5*A*, Table 1).

The $V_{½}$ of h_∞ for V930C and V930Q did not significantly differ from that of wild type, whereas V930A was hyperpolarized ($V_{½}$ = −91.3 ± 0.6 mV, $P < 0.001$) compared with hNa$_v$1.5 ($V_{½}$ = −80.7 ± 0.7 mV). The slopes of the h_∞ curves for V930A, V930C, and V930Q (k = 7.6 ± 0.3, $P < 0.001$; 7.4 ± 0.3, $P < 0.01$; and 7.6 ± 0.5, $P < 0.05$, respectively) were all less steep than that of hNa$_v$1.5 (k = 6.8 ± 0.4; Fig. 5*B*, Table 1).

Recovery From Short Depolarizations in V930A, V930C, and V930Q

When the mutants V930A, V930C, and V930Q were depolarized for 4 ms, recovery in V930C did not differ from that in hNa$_v$1.5 (τ = 2.1 ± 0.1 ms), whereas V930A and V930Q

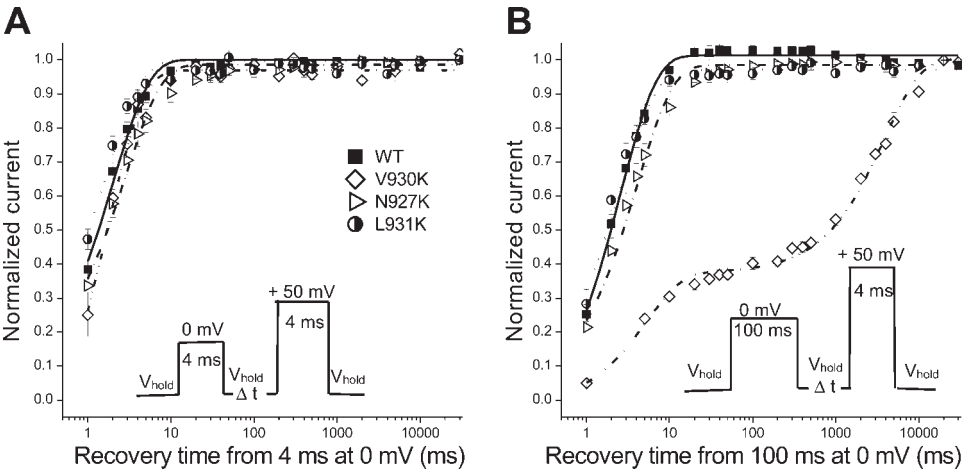

Fig. 3. Recovery from short depolarizations in hNa$_v$1.5 WT, N927K, V930K, and L931K. Recovery was determined with a test pulse (4 ms at +50 mV) after variable recovery times at the holding potential (V_{hold}) following a depolarization to 0 mV for 4 or 100 ms. *A*: recovery from 4-ms depolarization in mutants was similar to that in WT. Mean data were fit with a single-exponential function. *B*: recovery from a 100-ms depolarization was similar for WT compared with N927K and L931K (data fit with a single-exponential function). V930K exhibited a dramatically different biexponential time course of recovery, suggesting entry into a second distinct inactivated state within the 100-ms depolarization. Time constants are presented in Table 1.

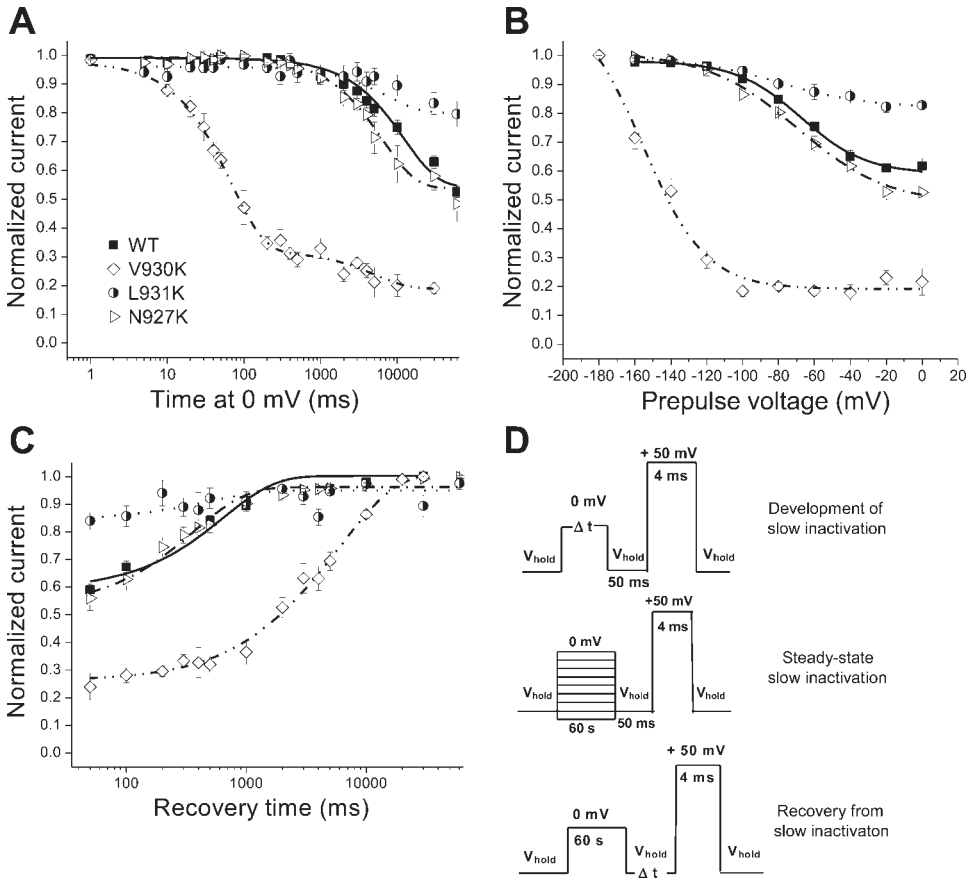

Fig. 4. Slow inactivation phenotypes for hNav1.5 WT, N927K, V930K, and L931K. The phenotype is defined as development of slow inactivation, steady-state slow inactivation (s_∞), and recovery from slow inactivation. Slow inactivation phenotype in N927K was similar to that of WT and L931K was somewhat resistant, whereas V930K had a greatly enhanced phenotype. *A*: slow inactivation was less complete in L931K than in WT, only showing ~17% after 60 s at 0 mV, whereas WT was ~45% inactivated. In contrast, V930K exhibited a dramatic enhancement of slow inactivation, with ~80% inactivation after a 30-s step to 0 mV. Mean data for development of slow inactivation were fit with a single- (WT, N927K, L931K) or double-exponential function (V930K). *B*: voltage dependence of s_∞ was similar in WT, N927K, and L931K, whereas V930K slow inactivated at much more hyperpolarized potentials. Mean data were fit with a Boltzmann function for s_∞ curves. *C*: recovery from slow inactivation in WT, N927K, and L931K were similar, although L931K recovered from less slow inactivation than the others. V930K shows a much slower and biexponential recovery compared with WT and the other mutants. Recovery data were fit with single-exponential functions (double-exponential for V930K). *D*: pulse protocols used in determining the slow inactivation phenotype. Data for slow inactivation phenotype are presented in Table 2.

recovered more slowly (τ = 3.1 ± 0.2 and 3.0 ± 0.2 ms, respectively, $P < 0.01$; Table 1). After a 100-ms depolarization, V930A recovered more slowly (τ = 3.4 ± 0.2 ms, $P < 0.001$) than wild type (τ = 2.6 ± 0.1 ms). Interestingly, after a 100-ms depolarization, V930Q exhibited a substantially slower and biexponential recovery (τ_1 = 5.6 ± 0.3 ms; τ_2 = 42.9 ± 4.6 ms) compared with hNa$_v$1.5 (Fig. 6, Table 1).

Slow Inactivation Phenotype in V930A, V930C, and V930Q

When we characterized the slow inactivation phenotype in V930A, V930C, and V930Q, we found that time constants for development of slow inactivation in V930A and V930C did not significantly differ from that of wild type. However, these mutants underwent less inactivation after 60 s at 0 mV (27 and 19%, respectively) than hNa$_v$1.5, which showed ~45% slow inactivation after this time (Fig. 7*A*). Development of slow inactivation in V930Q, as observed in V930K, was biexponential (τ1 = 395.2 ± 38.4 ms and τ2 = 14.8 ± 4.0 s) and much more complete (~80% after 60 s at 0 mV) than that of wild type (Fig. 7*A*, Table 2).

The s_∞ curve for V930Q is hyperpolarized ($V_{½}$ = −93.1 ± 1.6 mV, $P < 0.001$) and more steep (k = 10.0 ± 1.0, $P < 0.001$) compared with wild type ($V_{½}$ = −67.5 ± 3.2 mV, k = 18.2 ± 2.8). The s_∞ curve for V930C was also hyperpolarized

Table 2. *Comparison of slow inactivation phenotypes for hNa$_v$1.5 and mutant channels*

	Development of Slow Inactivation	Steady-State Slow Inactivation		Recovery From Slow Inactivation
	τ	$V_{1/2}$, mV	k	τ
hNa$_v$1.5	12.4±1.5 s (10)	−67.5±3.2 (19)	18.2±2.8	642.1±58.1 ms (12)
N927K	6.5±0.9 s (8)	−69.6±3.4 (6)	25.4±4.6	365.2±47.6 ms (8)
V930K	67.2±6.3 ms (66%) 5.1±2.3 s (13%) (5)	−155.6±7.5‡ (6)	17.5±4.1*	1.3±2.6 s (9%) 6.6±1.5 s (65%) (5)
L931K	19.8±14.5 s (9)	−79.2±9.2 (7)	23.7±9.5	481.0±350.8 ms (6)
V930A	8.5±0.7 s (21)	−75.4±2.8 (24)	26.5±2.4‡	313.6±55.2 ms (25)
V930C	9.5±2.0 s (6)	−100.4±3.3‡ (16)	12.1±2.2	144.1±87.4 ms (9)
V930Q	395.2±38.4 ms (51%) 14.8±4.0 s (30%) (13)	−93.1±1.6‡ (13)	10.0±1.0†	213.6±53.6 ms (49%) 7.4±1.5 s (39%) (13)

Steady-state slow inactivation curves were fit with a Boltzmann function. $V_{½}$ and k are means ± SE; numbers in parentheses are the number of cells recorded. Recovery and development curves were fit with either single- or double-exponential functions, and time constants (τ) are means ± SE; percentages are component of fit. *$P < 0.05$; †$P < 0.01$; ‡$P < 0.001$ compared with wild-type hNa$_v$1.5.

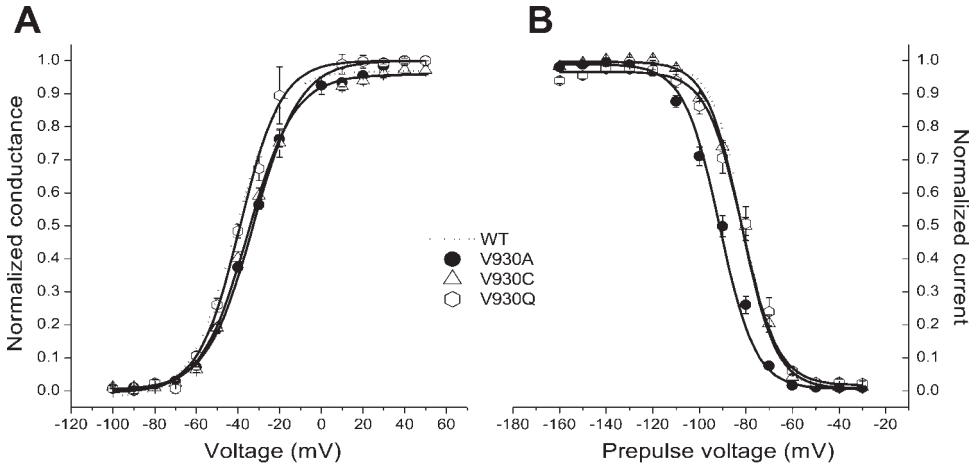

Fig. 5. Activation and h_∞ curves for V930A, V930C, and V930Q. See Fig. 1 for protocols. Mean data were fit with a Boltzmann function. *A*: the activation curves for V930A, V930C, and V930Q were all shifted in the depolarized direction compared with WT. *B*: steady-state h_∞ curves for V930C and V930Q were similar to that for WT, whereas the $V_{½}$ for V930A was hyperpolarized. The slopes of the h_∞ curves for V930A, V930C, and V930Q were all less steep than that for WT. Data are presented in Table 1.

($V_{½} = -100.4 \pm 3.3$ mV, $P < 0.001$; $k = 12.1 \pm 2.2$), and that of V930A ($k = 26.5 \pm 2.4$, $P < 0.001$) was less steep than that of hNa$_v$1.5 (Fig. 7*B*, Table 2).

The time constants of recovery from slow inactivation in V930A and V930C did not significantly differ from that in wild type, although these mutants were recovering from less inactivation than hNa$_v$1.5. Recovery of V930Q, as observed in V930K, was slower and biexponential with $\tau 1 = 213.6 \pm 53.6$ ms and $\tau 2 = 7.4 \pm 1.5$ s (Fig. 7*C*, Table 2).

DISCUSSION

In this study, we examined effects of amino acid substitutions in D2-S6 of the human cardiac Na^+ channel isoform hNa$_v$1.5, which is relatively resistant to slow inactivation, to further understand the role of this region in cardiac Na$_v$ slow inactivation phenotype (29, 35). Initially, we studied the mutant V930K, in which lysine is substituted for the native valine at residue 930 in D2-S6 of hNa$_v$1.5. We found that slow inactivation in this mutant was greatly enhanced, similar to that seen in the homologous mutant V787K of rNa$_v$1.4 (30). To determine whether the effect of lysine substitution was specific to the V930 site, we studied two additional lysine-substituted mutants at nearby sites in D2-S6, N927K and L931K, which did not show enhancement of slow inactivation. To determine whether enhanced slow inactivation in V930K is dependent on the specific amino acid substitution (i.e., lysine), we recorded from three other mutants with substitutions at this position: V930A (alanine), V930C (cysteine), and V930Q (glutamine). We found that glutamine substitution (V930Q) also showed the enhanced slow inactivation phenotype, but other substitutions at V930 (V930A and V930C) did not. In general, V930A, V930C, and L931K demonstrated a reduced slow inactivation phenotype.

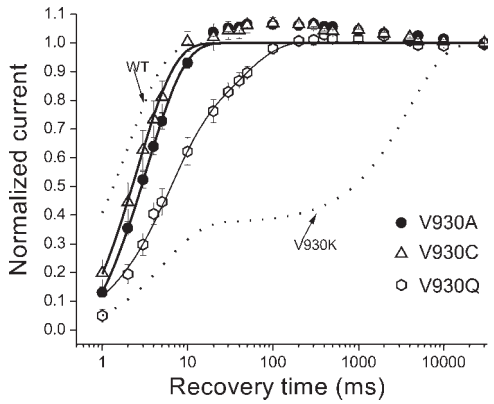

Fig. 6. Recovery from short depolarization in V930A, V930C, and V930Q. See Fig. 3 for protocols. Recovery from 100-ms depolarization for V930C and V930A was comparable to that for WT, whereas recovery in V930Q was delayed. Recovery curve for V930K is shown for comparison. Mean data were fit with a single-exponential function for V930A and V930C and a biexponential function for V930Q. Time constants are presented in Table 1.

Several of the mutants studied showed changes in fast kinetics (activation and steady-state fast inactivation). For example, activation in all mutants except V927K was depolarized, and the curve was less steep in V930K. The steady-state fast inactivation curve (h_∞) was hyperpolarized in N927K, V930K, and V930A, whereas h_∞ was depolarized in L931K. Also, there was a decrease in the steepness of the steady-state fast inactivation curve in all mutants except N927K and L931K. It is not uncommon to see changes in slope or voltage shifts in these curves with amino acid substitutions in D2-S6 and other S6 segments (17, 30, 33, 51, 52, 53, 54, 57, 58). These changes in activation and steady-state fast inactivation did not affect our measurements of slow inactivation, because our slow inactivation protocols isolate the slow inactivation process from fast inactivation and activation variability. That is, our holding potentials (-160 or -180 mV) and test potential ($+50$ mV) ensured that the channels were available to open (i.e., not fast inactivated) and that they would open when depolarized (i.e., maximized open probability), regardless of shifts in fast inactivation and activation curves.

A potential concern with mutational effects on fast inactivation is that previous studies have shown a coupling between fast inactivation and slow inactivation (10, 24, 36). Specifically, these conclusions have been based on the observation that when fast inactivation is disrupted, slow inactivation is accelerated or enhanced. This is accomplished with internal perfusion with pronase (36) or mutagenesis directed at the D3-D4 loop, the presumed fast-inactivation gate or "lid" (10, 24). These methods result in Na^+ currents with a noninactivating component that reflects incomplete closure of the fast inactivation gate during open-state fast inactivation. The hypothesis is that blocking or eliminating entry into the fast-inactivated state drives channels more rapidly from the open

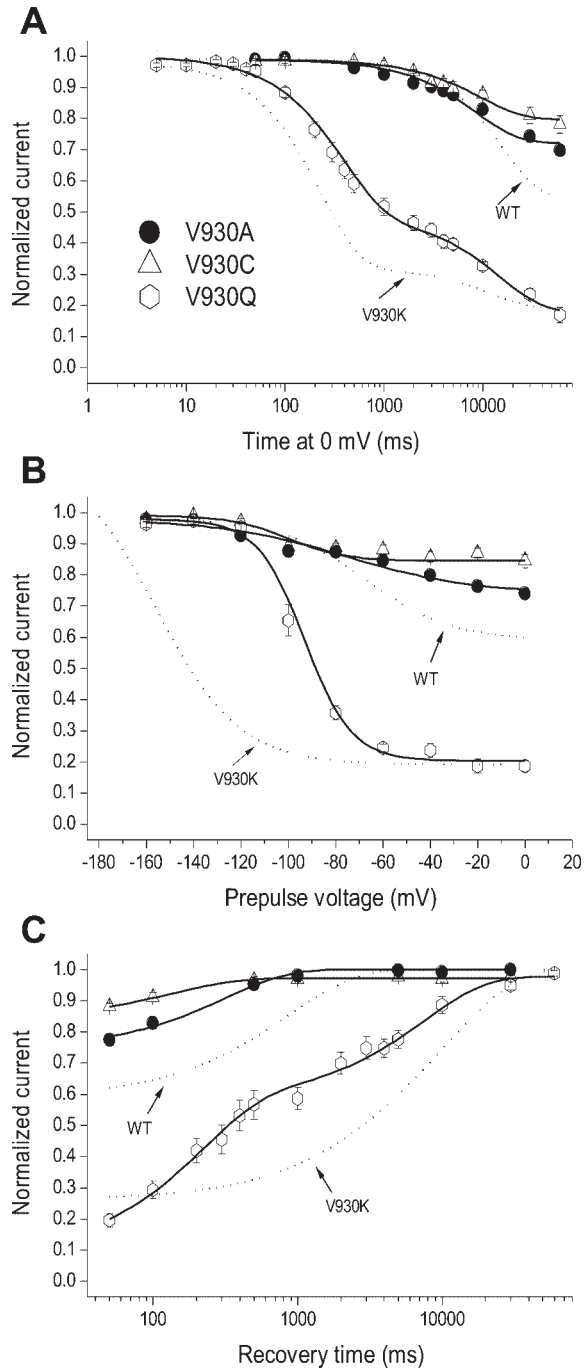

Fig. 7. Slow inactivation phenotype for mutants with substitutions at V930. See Fig. 4*D* for protocols. *A*: development of slow inactivation was similar to that in WT in V930A and V930C, although these mutants underwent less inactivation. After 60 s at 0 mV, V930C was ~19% inactivated and V930A was ~27% inactivated compared with 45% inactivation in WT. Curves were fit with a single-exponential function. Slow inactivation in V930Q developed faster, was greater in magnitude (80%), and was biexponential. *B*: the steady-state s_∞ curve of V930A was similar to that of WT, whereas the $V_{½}$ for V930C was hyperpolarized. The s_∞ curve of V930Q was also hyperpolarized and shows much greater slow inactivation at all potentials above −100 mV. Mean data were fit with a Boltzmann function. *C*: recovery from slow inactivation for V930C and V930A were similar in pattern to that for WT, although these mutants were recovering from less inactivation. V930Q required more time to recover from an enhanced slow inactivation state. Mean data were fit with a single- (V930A and V930C) or double-exponential function (V930Q). Data are presented in Table 2.

state into the slow-inactivated state (36). However, it is less clear whether changes in steady-state fast inactivation (closed-state fast inactivation) consistently produce changes in slow inactivation. For example, Wang et al. (53) found that some tryptophan or cysteine substitutions in D1-S6 or D4-S6 in rNa$_v$1.4 disrupted fast inactivation, producing a noninactivating current and an enhancement of slow inactivation. However, there was no consistent effect on the steady-state fast inactivation curve h_∞ in these mutants in this study. These inconsistencies also have been found in D2-S6 of rNa$_v$1.4 (17), and we found similar inconsistencies in our results in hNa$_v$1.5. None of our mutants exhibited noninactivating current components. Of the mutants with enhanced slow inactivation phenotypes, the h_∞ curve was hyperpolarized by −15 mV in V930K but was not affected in V930Q. Indeed, in V930A, which showed some resistance to slow inactivation, the h_∞ curve was hyperpolarized by −10 mV, similar to V930K, whereas in L931K, which also showed slow inactivation resistance, the h_∞ curve was depolarized by more than +10 mV. It should be noted that the slope of the h_∞ curve in V930K showed the greatest change (much less steep) compared with the other mutants. From the data in this study and others, it appears that mechanisms (or specific residues) associated with steady-state fast inactivation may not be tightly coupled to those of slow inactivation, or that certain substitutions may uncouple these two inactivation processes.

To further characterize inactivation in the mutants, we studied the recovery profile from a short (100 ms) depolarization to 0 mV, which only produces fast inactivation in wild-type hNa$_v$1.5. Most of the mutants were similar to wild type. However, V930K and V930Q showed a biphasic recovery from this short depolarization, suggesting that both mutants were rapidly entering an additional inactivated state, which we propose to be the slow-inactivated state. We then used our slow inactivation protocols to further characterize the slow inactivation phenotypes in the mutants.

Of the three lysine-substituted mutants (N927K, V930K, and L931K), only V930K exhibited enhanced slow inactivation. This suggests that the enhancement effect of lysine substitution is site specific to V930. Indeed, the L931K mutant with a lysine substitution adjacent to V930 exhibited resistance to slow inactivation, whereas the N927K mutant at a site three amino acids away from V930 (almost a turn of the helix) closely resembled wild-type hNa$_v$1.5. It is likely that effects of lysine substitutions on slow inactivation are due, at least in part, to differences in hydrophobicity between specific residues. For example, both valine and leucine are hydrophobic, whereas asparagine and lysine are hydrophilic (18). Therefore, one might expect normal slow inactivation gating to be altered when a native hydrophobic residue is replaced with a hydrophilic one (e.g., V930K or L931K), whereas replacing a native hydrophilic residue with another hydrophilic one would have less of an effect (e.g., N927K). A possible explanation for these results is that during the conformational changes underlying slow inactivation, the V930 residue moves toward a more hydrophilic microenvironment (e.g., water-filled cavity or pore) and the L931 residue moves toward a more hydrophobic microenvironment (e.g., membrane or within the protein). Therefore, the lysine substitution in V930K would favor slow inactivation conformational changes, whereas the L931K would be more resistant. Furthermore, the resistance observed

in L931K might be influenced by lysine side-chain positioning adjacent to that of asparagine at N932. The contiguous placement of two strongly hydrophilic residues may alter or restrict conformational changes in the channel necessary for slow inactivation (e.g., around V930). Consistent with a slow inactivation model that includes molecular rearrangement in this region are studies demonstrating slow inactivation-induced accessibility of cysteine substitution in V930C in hNa$_v$1.5 and the homologous rNa$_v$1.4 mutant V787C (28, 30). Thus molecular movement involving residue V930 appears to play an important role in slow inactivation gating in both Na$_v$ isoforms, a conclusion strengthened by data from the present study.

In addition to the lysine substitutions, we studied other amino acids at the V930 site to determine whether the enhancement effect on slow inactivation was residue specific as well as site specific. Of the mutants examined, V930A (alanine), V930C (cysteine), and V930Q (glutamine) expressed sufficient current for analysis. Recordings from V930A, V930C, and V930Q determined that only V930Q had an enhanced slow inactivation phenotype, similar to V930K, whereas V930A and V930C did not. One explanation for these results is that because glutamine is similar in hydrophobicity to lysine (18), the enhancement effect in V930Q could be due primarily to the change from the hydrophobic valine to the more hydrophilic glutamine. The greater enhancement of steady-state slow inactivation (more hyperpolarized s_∞ curve) seen in V930K relative to V930Q likely derives from the larger size and/or positive charge on lysine, which may further promote or stabilize conformational changes associated with slow inactivation. Further information about effects of the charged side chain in lysine might come from other charged amino acid substitutions. However, we produced two mutants with charged side chains, V930R and V930D, but neither of these mutants expressed adequate current, which could be due to problems such as intracellular trafficking, folding, or function.

The A and C substitutions in V930A and V930C are somewhat smaller (34) and less hydrophobic than the native valine (18), and these mutants exhibit a resistance to slow inactivation (similar to L931K). Perhaps small reductions in hydrophobicity at this position, while not enhancing conformations that favor slow inactivation, promote a conformation from which slow inactivation is more difficult. For example, A or C may cause a small shift in the position of the side chain, thus preventing molecular interactions necessary to trigger the slow inactivated conformation. In regard to relative size of the amino acid substitutions at V930, A and C, which are smaller than V, do not enhance slow inactivation, whereas K and Q, which are larger than V, do show enhancement, demonstrating that larger, more hydrophilic residues at this position enhance slow inactivation. We do not believe that D2-S6 helix disruption explains our results because, although cysteine might be expected to destabilize the α-helix relative to the native valine, lysine (at any of the positions studied), glutamine, or alanine would not (8). Collectively, these results suggest that molecular rearrangement involving V930 is critical for slow inactivation and involves movement of residues within microenvironments that have hydrophobicity and/or size constraints for normal function.

As mentioned previously, wild-type hNa$_v$1.5 is relatively resistant to slow inactivation compared with wild-type rNa$_v$1.4. The enhanced slow inactivation phenotype seen in the V930K mutant of hNa$_v$1.5 is similar to the enhancement seen with the homologous lysine substitution in V787K of rNa$_v$1.4 (30). This suggests that different Na$_v$ isoforms share some molecular components (and mechanisms) of slow inactivation despite different overall slow inactivation phenotypes. However, enhancement of slow inactivation in hNa$_v$1.5-V930K appears to be greater than that in rNa$_v$1.4-V787K (compare 185-fold acceleration in major component of development, 35% increase in slow-inactivated current, and hyperpolarizing shift in $V_{½}$ of −88 mV in hNa$_v$1.5-V930K vs. 90-fold acceleration in major component of development, 10% increase in slow-inactivated current, and hyperpolarizing shift in $V_{½}$ of −53 mV in rNa$_v$1.4-V787K; Ref. 30). It is possible that lysine (and glutamine) substitutions at this position have comparable positive effect(s) on slow inactivation in both isoforms but that the greater effect seen in hNa$_v$1.5-V930K derives from structural differences between the channels. rNa$_v$1.4 appears to normally favor conformational changes involving D2-S6 during slow inactivation. This is supported by data from previous studies demonstrating that molecular movement at V787/930 in D2-S6 during Na$_v$ slow inactivation (as monitored by MTS modification) occurs more readily in rNa$_v$1.4 (30) than in hNa$_v$1.5 (28). Thus rNa$_v$1.4 might be expected to show less enhancement with these substitutions than hNa$_v$1.5.

The enhanced effect in hNa$_v$1.5 may also relate to structures and/or mechanisms in the heart Na$_v$ channel that have evolved to limit slow inactivation in heart muscle. Indeed, enhanced slow inactivation of Na$_v$s during prolonged cardiac action potentials would probably be lethal, or at least selected against. It is possible that areas within hNa$_v$1.5 negatively regulate slow inactivation, and disruption of this regulation by the V930K (or Q) mutation disinhibits the inherent suppression. This would confer an additional enhancement of slow inactivation with these mutations in hNa$_v$1.5 that is not seen in rNa$_v$1.4. Candidate areas for structural differences in Na$_v$s that vary between isoforms and may contribute to isoform-specific differences in response to mutations in D2-S6 include P-loops, other S6 segments, and possibly intracellular loops between domains (e.g., D1-D2 or D2-D3).

Interaction between different regions of Na$_v$s during slow inactivation was proposed in a recent study by Wang et al. (55). In their study, lysine or tryptophan (W) substitution at S1759 in D4-S6 of hNa$_v$1.5, the putative "gating hinge" in this domain (59), produced an enhancement of slow inactivation at negative potentials (55). The authors proposed that slow inactivation enhancement in S1759K and S1759W may involve interaction of this gating-hinge residue with the DEKA locus of the selectivity filter in the P-loop. In our study, the V930 residue in D2-S6 is four amino acids below (toward the intracellular side of the channel) the glycine gating hinge in D2 (G926), so we believe it is unlikely that V930 interacts directly with the P-loop during slow inactivation gating. However, we cannot rule out interactions (direct or indirect) with other regions of the channel that would influence local gating mechanisms near the V930 site. Interestingly, the N927K mutant studied presently, which has lysine substituted adjacent to the G926 gating-hinge residue, showed no change in slow inactivation phenotype compared with wild type. It may be that S6 segments in different domains play different roles in slow inactivation or that other sites in S6, in addition to the gating hinge, contribute to slow inactivation gating.

In conclusion, we have shown that substitution of lysine or glutamine at V930 in D2-S6 of hNa$_v$1.5 dramatically reverses the relative resistance to slow inactivation normally seen in cardiac Na^+ channels. The effects on slow inactivation of substitutions in this study can be explained by differences in amino acid hydrophobicity and/or size that influence requisite molecular movements. Although Na$_v$ slow inactivation is a complex process likely involving several regions of the protein, we suggest that molecular movement in D2-S6 at or near V930 is a critical component of slow inactivation that is shared between isoforms, but isoforms can differ in their ability to undergo conformational changes in this region, partially explaining isoform-specific slow inactivation phenotypes.

ACKNOWLEDGMENTS

We thank Dr. Ted Cummins, Indiana University School of Medicine, Indianapolis, IN, for the hNav1.5 clone; Dr. Sho-Ya Wang, SUNY Albany, Albany, NY, for the V930K and V930C mutants; Jodi Johnson, Southeastern Louisiana University, Hammond, LA, for work on the lysine-substituted mutants; and Dr. Al Goldin, University of California, Irvine, CA, for supplying Nav sequence information.

GRANTS

This study was supported by Faculty Development Grants from the Center for Faculty Excellence at Southeastern Louisiana University and by National Heart, Lung, and Blood Institute Grant R15 HL080009-01.

REFERENCES

1. **Antzelevitch C, Brugada P, Brugada J, Brugada R.** Brugada syndrome: from cell to bedside. *Curr Probl Cardiol* 30: 9–54, 2005.
2. **Antzelevitch C, Brugada P, Brugada J, Brugada R, Shimizu W, Gussak I, Perez Riera AR.** Brugada syndrome: a decade of progress. *Circ Res* 91: 1114–1118, 2002.
3. **Balser JR, Nuss HB, Chiamvimonvat N, Perez-Garcia MT, Marban E, Tomaselli GF.** External pore residue mediates slow inactivation in mu 1 rat skeletal muscle sodium channels. *J Physiol* 494: 431–442, 1996.
4. **Benitah JP, Chen Z, Balser JR, Tomaselli GF, Marban E.** Molecular dynamics of the sodium channel pore vary with gating: interactions between P-segment motions and inactivation. *J Neurosci* 19: 1577–1585, 1999.
5. **Brugada P, Brugada R, Antzelevitch C, Brugada J.** The Brugada Syndrome. *Arch Mal Coeur Vaiss* 98: 115–122, 2005.
6. **Cannon SC.** Pathomechanisms in channelopathies of skeletal muscle and brain. *Annu Rev Neurosci* 29: 387–415, 2006.
7. **Chen Y, Yu FH, Surmeier DJ, Scheuer T, Catterall WA.** Neuromodulation of Na^+ channel slow inactivation via cAMP-dependent protein kinase and protein kinase C. *Neuron* 49: 409–420, 2006.
8. **Chou PY, Fasman GD.** Prediction of protein conformation. *Biochemistry* 13: 222–245, 1974.
9. **Cota G, Armstrong CM.** Sodium channel gating in clonal pituitary cells. The inactivation step is not voltage dependent. *J Gen Physiol* 94: 213–232, 1989.
10. **Featherstone DE, Richmond JE, Ruben PC.** Interaction between fast and slow inactivation in Skm1 sodium channels. *Biophys J* 71: 3098–3109, 1996.
11. **Fozzard HA, Hanck DA.** Structure and function of voltage-dependent sodium channels: comparison of brain II and cardiac isoforms. *Physiol Rev* 76: 887–926, 1996.
12. **Gellens ME, George AL Jr, Chen LQ, Chahine M, Horn R, Barchi RL, Kallen RG.** Primary structure and functional expression of the human cardiac tetrodotoxin-insensitive voltage-dependent sodium channel. *Proc Natl Acad Sci USA* 89: 554–558, 1992.
13. **Graham FL, Eb AJ.** A new technique for the assay of infectivity of human adenovirus 5 DNA. *Virology* 52: 456–467, 1973.
14. **Hamill OP, Marty A, Neher E, Sakmann B, Sigworth FJ.** Improved patch-clamp techniques for high-resolution current recording from cells and cell-free membrane patches. *Pflügers Arch* 391: 85–100, 1981.
15. **Hoshi T, Zagotta WN, Aldrich RW.** Two types of inactivation in Shaker K^+ channels: effects of alterations in the carboxy-terminal region. *Neuron* 7: 547–556, 1991.
16. **Itoh H, Tsuji K, Sakaguchi T, Nagaoka I, Oka Y, Nakazawa Y, Yao T, Jo H, Ashihara T, Ito M, Horie M, Imoto K.** A paradoxical effect of lidocaine for the N406S mutation of SCN5A associated with Brugada syndrome. *Int J Cardiol* 121: 239–248, 2007.
17. **Kondratiev A, Tomaselli GF.** Altered gating and local anesthetic block mediated by residues in the I-S6 and II-S6 transmembrane segments of voltage-dependent Na^+ channels. *Mol Pharmacol* 64: 741–752, 2003.
18. **Kyte J, Doolittle RF.** A simple method for displaying the hydropathic character of a protein. *J Mol Biol* 157: 105–132, 1982.
19. **Liu Y, Jurman ME, Yellen G.** Dynamic rearrangement of the outer mouth of a K^+ channel during gating. *Neuron* 16: 859–867, 1996.
20. **McPhee JC, Ragsdale DS, Scheuer T, Catterall WA.** A critical role for the S4-S5 intracellular loop in domain IV of the sodium channel α-subunit in fast inactivation. *J Biol Chem* 273: 1121–1129, 1998.
21. **Meisler MH, Kearney JA.** Sodium channel mutations in epilepsy and other neurological disorders. *J Clin Invest* 115: 2010–2017, 2005.
22. **Napolitano C, Priori SG.** Brugada syndrome. *Orphanet J Rare Dis* 1: 35, 2006.
23. **Noda M, Ikeda T, Suzuki H, Takeshima H, Takahashi T, Kuno M, Numa S.** Expression of functional sodium channels from cloned cDNA. *Nature* 322: 826–828, 1986.
24. **Nuss HB, Balser JR, Orias DW, Lawrence JH, Tomaselli GF, Marban E.** Coupling between fast and slow inactivation revealed by analysis of a point mutation (F1304Q) in mu 1 rat skeletal muscle sodium channels. *J Physiol* 494: 411–429, 1996.
25. **Ogielska EM, Zagotta WN, Hoshi T, Heinemann SH, Haab J, Aldrich RW.** Cooperative subunit interactions in C-type inactivation of K channels. *Biophys J* 69: 2449–2457, 1995.
26. **O'Leary ME.** Characterization of the isoform-specific differences in the gating of neuronal and muscle sodium channels. *Can J Physiol Pharmacol* 76: 1041–1050, 1998.
27. **Ong BH, Tomaselli GF, Balser JR.** A structural rearrangement in the sodium channel pore linked to slow inactivation and use dependence. *J Gen Physiol* 116: 653–662, 2000.
28. **O'Reilly JP, Shockett PE.** Slow-inactivation induced conformational change in domain 2-segment 6 of cardiac Na^+ channel. *Biochem Biophys Res Commun* 345: 59–66, 2006.
29. **O'Reilly JP, Wang SY, Kallen RG, Wang GK.** Comparison of slow inactivation in human heart and rat skeletal muscle Na channel chimeras. *J Physiol* 515: 61–73, 1999.
30. **O'Reilly JP, Wang SY, Wang GK.** Residue-specific effects on slow inactivation at V787 in D2-S6 of Na$_v$1.4 sodium channels. *Biophys J* 81: 2100–2111, 2001.
31. **Panyi G, Sheng Z, Deutsch C.** C-type inactivation of a voltage-gated K^+ channel occurs by a cooperative mechanism. *Biophys J* 69: 896–903, 1995.
32. **Patton DE, West JW, Catterall WA, Goldin AL.** Amino acid residues required for fast Na^+-channel inactivation: charge neutralizations and deletions in the III-IV linker. *Proc Natl Acad Sci USA* 89: 10905–10909, 1992.
33. **Ragsdale DS, McPhee JC, Scheuer T, Catterall WA.** Molecular determinants of state-dependent block of Na^+ channels by local anesthetics. *Science* 265: 1724–1728, 1994.
34. **Richards FM.** The interpretation of protein structures: total volume, group volume distributions and packing density. *J Mol Biol* 82: 1–14, 1974.
35. **Richmond JE, Featherstone DE, Hartmann HA, Ruben PC.** Slow inactivation in human cardiac sodium channels. *Biophys J* 74: 2945–2952, 1998.
36. **Rudy B.** Slow inactivation of the sodium conductance in squid giant axons. Pronase resistance. *J Physiol* 283: 1–21, 1978.
37. **Rush AM, Cummins TR, Waxman SG.** Multiple sodium channels and their roles in electrogenesis within dorsal root ganglion neurons. *J Physiol* 579: 1–14, 2007.
38. **Sasaki K, Makita N, Sunami A, Sakurada H, Shirai N, Yokoi H, Kimura A, Tohse N, Hiraoka M, Kitabatake A.** Unexpected mexiletine responses of a mutant cardiac Na^+ channel implicate the selectivity filter as a structural determinant of antiarrhythmic drug access. *Mol Pharmacol* 66: 330–336, 2004.
39. **Shirai N, Makita N, Sasaki K, Yokoi H, Sakuma I, Sakurada H, Akai J, Kimura A, Hiraoka M, Kitabatake A.** A mutant cardiac sodium channel with multiple biophysical defects associated with overlapping clinical features of Brugada syndrome and cardiac conduction disease. *Cardiovasc Res* 53: 348–354, 2002.

40. **Smith MR, Goldin AL.** Interaction between the sodium channel inactivation linker and domain III S4-S5. *Biophys J* 73: 1885–1895, 1997.
41. **Struyk AF, Cannon SC.** Slow inactivation does not block the aqueous accessibility to the outer pore of voltage-gated Na channels. *J Gen Physiol* 120: 509–516, 2002.
42. **Tikhonov D, Zhorov BS.** Sodium channels: ionic model of slow inactivation and state-dependent drug binding. *Biophys J* 93: 1557–1570, 2007.
43. **Ukomadu C, Zhou J, Sigworth FJ, Agnew WS.** μ1 Na^+ channels expressed transiently in human embryonic kidney cells: biochemical and biophysical properties. *Neuron* 8: 663–676, 1992.
44. **Vedantham V, Cannon SC.** Rapid and slow voltage-dependent conformational changes in segment IVS6 of voltage-gated Na^+ channels. *Biophys J* 78: 2943–2958, 2000.
45. **Veldkamp MW, Viswanathan PC, Bezzina C, Baartscheer A, Wilde AA, Balser JR.** Two distinct congenital arrhythmias evoked by a multidysfunctional Na^+ channel. *Circ Res* 86: E91–E97, 2000.
46. **Vilin YY, Fujimoto E, Ruben PC.** A single residue differentiates between human cardiac and skeletal muscle Na^+ channel slow inactivation. *Biophys J* 80: 2221–2230, 2001.
47. **Vilin YY, Ruben PC.** Slow inactivation in voltage-gated sodium channels: molecular substrates and contributions to channelopathies. *Cell Biochem Biophys* 35: 171–190, 2001.
48. **Viswanathan PC, Balser JR.** Inherited sodium channelopathies: a continuum of channel dysfunction. *Trends Cardiovasc Med* 14: 28–35, 2004.
49. **Wang DW, Makita N, Kitabatake A, Balser JR, George AL Jr.** Enhanced Na^+ channel intermediate inactivation in Brugada syndrome. *Circ Res* 87: E37–E43, 2000.
50. **Wang DW, Viswanathan PC, Balser JR, George AL Jr, Benson DW.** Clinical, genetic, and biophysical characterization of SCN5A mutations associated with atrioventricular conduction block. *Circulation* 105: 341–346, 2002.
51. **Wang SY, Barile M, Wang GK.** Disparate role of Na^+ channel D2-S6 residues in batrachotoxin and local anesthetic action. *Mol Pharmacol* 59: 1100–1107, 2001.
52. **Wang SY, Barile M, Wang GK.** A phenylalanine residue at segment D3-S6 in Nav1.4 voltage-gated Na^+ channels is critical for pyrethroid action. *Mol Pharm* 60: 620–628, 2001.
53. **Wang SY, Bonner K, Russell C, Wang GK.** Tryptophan scanning of D1S6 and D4S6 C-termini in voltage-gated sodium channels. *Biophys J* 85: 911–920, 2003.
54. **Wang SY, Nau C, Wang GK.** Residues in Na^+ channel D3-S6 segment modulate both batrachotoxin and local anesthetic affinities. *Biophys J* 79: 1379–1387, 2000.
55. **Wang SY, Russell C, Wang GK.** Tryptophan substitution of a putative D4S6 gating hinge alters slow inactivation in cardiac sodium channels. *Biophys J* 88: 3991–3999, 2005.
56. **Wang SY, Wang GK.** A mutation in segment I-S6 alters slow inactivation of sodium channels. *Biophys J* 72: 1633–1640, 1997.
57. **Yarov-Yarovoy V, Brown J, Sharp EM, Clare JJ, Scheuer T, Catterall WA.** Molecular determinants of voltage-dependent gating and binding of pore-blocking drugs in transmembrane segment IIIS6 of the Na^+ channel alpha subunit. *J Biol Chem* 276: 20–27, 2001.
58. **Yarov-Yarovoy V, McPhee JC, Idsvoog D, Pate C, Scheuer T, Catterall WA.** Role of amino acid residues in transmembrane segments IS6 and IIS6 of the Na^+ channel alpha subunit in voltage-dependent gating and drug block. *J Biol Chem* 277: 35393–35401, 2002.
59. **Zhao Y, Yarov-Yarovoy V, Scheuer T, Catterall WA.** A gating hinge in Na^+ channels; a molecular switch for electrical signaling. *Neuron* 41: 859–865, 2004.